ACS Catalysis

Research Article

pubs.acs.org/acscatalysis

Carbon Support Surface Effects in the Gold-Catalyzed Oxidation of 5-Hydroxymethylfurfural

Baira Donoeva,* Nazila Masoud, and Petra E. de Jongh*

Inorganic Chemistry and Catalysis, Debye Institute for Nanomaterials Science, Utrecht University, Universiteitsweg 99, 3584 CG Utrecht, The Netherlands

Supporting Information

ABSTRACT: Oxidation of 5-hydroxymethylfurfural into 2,5-furandicarboxylic acid is an important transformation for the production of bio-based polymers. Carbon-supported gold catalysts hold great promise for this transformation. Here we demonstrate that the activity, selectivity, and stability of the carbon-supported gold nanoparticles in the oxidation of 5-hydroxymethylfurfural strongly depend on the surface properties of the carbon support. Gold nanoparticles supported on basic carbon materials with a low density of functional groups demonstrate higher activity in 5-hydroxymethylfurfural oxidation (TOF_{Au} up to 1195 h^{-1}), higher selectivity to 2,5-furandicarboxylic acid, and better stability in comparison to gold nanoparticles supported on carbon materials with acidic surface groups. Surface groups of basic carbon supports that are positively charged under the reaction conditions result in a higher adsorption and local concentration of hydroxyl ions, which act as cocatalysts for gold and enhance gold-catalyzed dehydrogenation. Negatively charged surface groups of acidic carbons repel hydroxyls and the intermediate monoacid anions, which leads to lower reaction rates and a high selectivity toward 2,5-hydroxymethylfurancarboxylic acid. Understanding the role of support surface charge and local hydroxyl anion concentration provides a basis for the rational design of the optimal carbon support surface chemistry for highly active, selective, and stable catalysts for the oxidation of 5-hydroxymethylfurfural and related reactions.

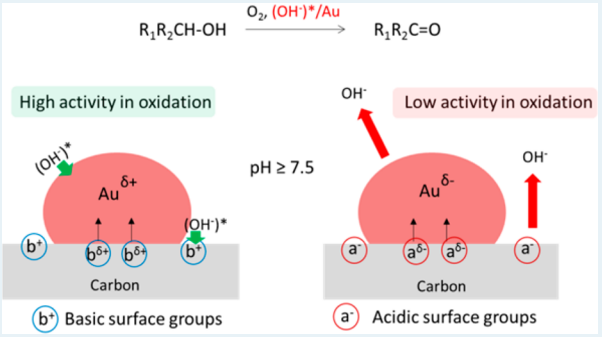

KEYWORDS: *selective oxidation, gold nanoparticles, carbon, surface functionalization, 5-hydroxymethylfurfural*

INTRODUCTION

Transformation of biomass into chemicals represents a promising way to reduce our society's dependence on nonrenewable resources as well as the environmental impact associated with the use of fossil resources. Recent advances in the transformation of biomass polymers, such as cellulose and hemicellulose, open novel possibilities for obtaining value-added chemicals from renewable resources.[1,2] For example, 5-hydroxymethylfurfural (HMF), a platform chemical derived from sugars, contains hydroxymethyl and carbonyl groups which can be oxidized to form various important furanic chemicals (Scheme 1), such as diformylfuran (DFF), 2,5-hydroxymethylfurancarboxylic acid (HMFCA), 2,5-formylfurancarboxylic acid (FFCA), and 2,5-furandicarboxylic acid (FDCA). FDCA has recently attracted major interest because it can serve as a renewable alternative to terephthalic acid in the production of polymers, a precursor in organic synthesis, and a building block for metal−organic framework materials.[3]

Substantial progress has been achieved in the conversion of HMF to FDCA using air or molecular oxygen as an oxidant, catalyzed by supported metal catalysts such as Au, Ru, Pt, Pd, and bimetallics in aqueous media.[4−9] In particular, supported gold catalysts have attacted considerable interest due to their high activity in the oxidation of HMF to FDCA and resistance to oxide formation, which is believed to be one of the main causes of catalyst deactivation for other metals. The mechanism of alcohol oxidation over supported metal catalysts in basic aqueous media was investigated by Davis and co-workers.[10−12] The results indicate that water is the source of oxygen atoms in the products of HMF oxidation, while dehydrogenation steps are catalyzed by hydroxyls adsorbed on the Au surface. Molecular O_2 closes the redox cycle by removing negative charge formed during hydrogen abstraction from the metal nanoparticles, thus regenerating the consumed hydroxyls.[13]

Carbon materials are promising catalyst supports for metal nanoparticles, in particular for fuel cell catalysts and catalysis in the aqueous phase, due to their high stability in aqueous media over a broad pH range, the possibility of full recovery of expensive metals via support combustion, and the ease of surface functionalization by incorporating other elements, such as oxygen and nitrogen.[14,15] Various methods to introduce oxygen- or nitrogen-containing surface functional groups have been employed.[16−18] These functional groups can be acidic, basic, or neutral (Figure 1), and their concentrations and

Received: March 15, 2017
Revised: May 9, 2017
Published: May 31, 2017

DOI: 10.1021/acscatal.7b00829
ACS Catal. 2017, 7, 4581−4591

Scheme 1. Oxidation of HMF to FDCA

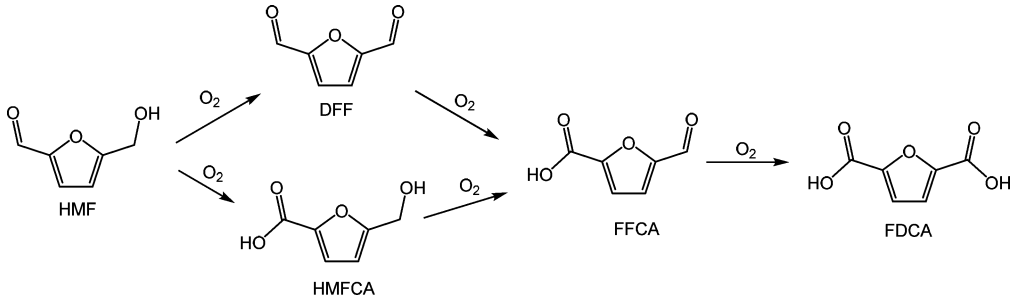

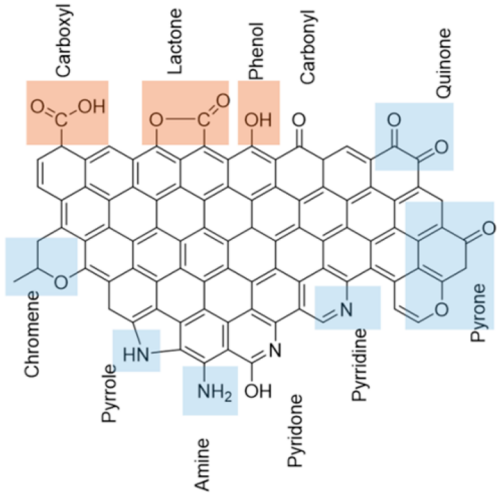

Figure 1. Selected possible functional groups on the surface of carbon materials. Acidic groups are highlighted in red, and basic groups are highlighted in blue.

strengths determine the overall acidity/basicity of the material. The point of zero charge (PZC) of carbon materials can be tuned over a broad range. Carbon materials free of surface functional groups are known to be hydrophobic/nonpolar; therefore, surface functionalization is often required for the catalyst preparation to improve carbon surface wetting properties and thus obtain catalysts with high metal loadings and small particle sizes.[18,15,19]

Previous studies of carbon-supported metal catalysts show that carbon surface properties influence the size and distribution of supported metal nanoparticles as well as catalyst performance, as was summarized in an excellent review by Prati et al.[20] However, in some cases it was not possible to ascribe the observed catalytic effects to carbon surface properties exclusively, since catalysts with different metal particle sizes and distributions were compared. Colloidal nanoparticles are often used to obtain catalysts with similar particle sizes irrespective of the support used.[21,22] In some recent studies, details of which are given below, catalysts prepared using metal colloids were used to investigate specifically the effect of the surface properties in aqueous-phase oxidation reactions.

Oxidation of Glycerol. Órfão and co-workers studied the effect of the surface properties of activated carbon (AC) and carbon nanotubes (CNT) on the activity of gold catalysts in the oxidation of glycerol.[23,24] The catalysts were prepared by immobilizing preformed colloidal gold nanoparticles on AC and CNT with different densities of oxygen-containing groups. Although the size of the final supported nanoparticles varied from 4.4 to 12.5 nm, it was possible to conclude that catalysts supported on carbons with a lower density of oxygen-containing groups were more active than catalysts supported on carbons with a high density of oxygenated groups.[12] Catalyst deactivation due to the growth of gold nanoparticles on both AC and CNT during glycerol oxidation was reported. Prati et al. found that the activity and selectivity of gold nanoparticles with similar sizes (2.9−4.6 nm) supported on nitrogen-doped CNT and carbon nanofibers (CNF) in the oxidation of glycerol increased with carbon basicity.[25] Authors suggested that basic groups of the carbon support are involved in the rate-limiting activation of the C−H bond. Selectivity to C3 products was demonstrated to be higher for basic catalysts than for acidic catalysts. The presence of hydrophilic oxygen-containing groups was found to lead to the formation of H_2O_2, which cleaved the C−C bond, producing C2 and C1 products.

Oxidation of HMF. The performance of bimetallic AuPd nanoparticles supported on CNT pretreated with either 30 or 68% HNO_3 or 30% H_2O_2 was studied in HMF oxidation under base-free conditions.[26] It was found that carbonyl/quinone and phenol functional groups facilitated adsorption of HMF and intermediates on the catalyst, thus increasing the rate of the oxidation steps, while carboxylic groups were detrimental to the adsorption of HMF and intermediates onto the catalyst. However, it was not specified whether the adsorption of HMF and intermediates was on the metal nanoparticles or the support surface. A similar result was obtained by the same group for Pt catalysts supported on a series of CNT with different oxygen-containing functional groups.[27] No explanation was given on why the particular functional groups improve or suppress the adsorption of HMF or intermediates. Besson et al. showed that introduction of oxygen-containing groups on the surface of activated carbon and mesoporous carbon CMK-3 reduced the activity of supported ruthenium nanoparticles in HMF oxidation.[28] The observed decrease in activity was proposed to be due to the increase in carbon hydrophilicity, resulting in the competitive adsorption between water and substrate/intermediate molecules on the support surface. Introduction of nitrogen-containing groups showed either negative or no effect on catalyst activity. Davis and co-workers observed that the yield of FDCA in HMF oxidation after 24 h was 62% in the presence of Au nanoparticles supported on nitrogen-doped CNF-N and only 18% over Au nanoparticles supported on oxidized CNF and carbon black (C_{black}).[11] Performing the reaction in the physical mixture of Au/C_{black} and CNF-N gave the same result as that with Au/C_{black} alone, indicating that gold nanoparticles should be supported on CNF-N to produce a high yield of FDCA. The authors stated "at this point, we cannot explain definitively the observed synergy of Au on CNF-N for diacid formation but will continue to explore its origins".

DOI: 10.1021/acscatal.7b00829
ACS Catal. 2017, 7, 4581−4591

The main aim of the present work was to understand how and why the surface properties of carbon supports affect the activity and selectivity of gold catalysts in HMF oxidation. Au particle growth is often encountered under oxidative conditions in the liquid phase but rarely studied.[29−36] Therefore, investigation on how support surface properties affect Au particle stability in oxidation reactions could provide insights which will help mitigating deactivation of gold catalysts. We systematically investigated a series of 2−4 nm gold nanoparticles supported on high-surface-area graphite (HSAG) with different surface chemistries, but the same morphology, in HMF oxidation under mildly basic conditions. We demonstrate that the surface properties of the carbon supports strongly affect the activity, selectivity, and stability of gold catalysts.

EXPERIMENTAL SECTION

Materials. Polyvinylpyrrolidone (PVP, MW 29000), $NaBH_4$ (≥98%), $HAuCl_4$ (>49.0% Au), 5-hydroxymethylfurfural (HMF), furandicarboxylic acid (FDCA), and 5-hydroxymethyl-2-furancarboxylic acid (HMFCA) were purchased from SigmaAldrich. High-surface-area graphite (HSAG, 500 m^2/g, d_{pore} 5.4 nm) was kindly provided by Timcal Ltd. Methanol (99+ %, extra pure) was purchased from AcrosOrganics.

Carbon Modification. In order to modify surface properties of HSAG, three different treatments have been applied. Oxidized HSAG (HSAG-ox) was obtained by gas-phase oxidation with HNO_3 vapor using the procedure and a setup described elsewhere.[17] This treatment was reported to be highly effective for the introduction of various oxygen-containing functional groups on the surface of carbon nanotubes without significant change in their textural properties. Briefly, heated quartz sample holder (150 °C) containing 0.5 g of HSAG was connected to a reflux condenser and placed on top of a 1 L round-bottom flask containing 150 mL of concentrated nitric acid. The acid was heated to boiling, and the HSAG-ox was collected after 5 min of treatment.

Since the surface of the pristine HSAG already contained 5.6 atom % of oxygen (vide infra), reduction treatment was applied to remove a fraction of oxygen-containing groups. Hydrogen-treated HSAG (HSAG-H) was obtained by treating pristine HSAG in a flow of 20% H_2 in N_2 at a rate of 100 mL/min at 400 °C (heating rate 2 °C/min) for 12 h.

Finally, amination treatment of carbon materials, i.e. treatment with gaseous NH_3, was applied in order to incorporate nitrogen-containing functional groups on the carbon surface (HSAG-N) by treating the pristine HSAG with gaseous NH_3 at 600 °C and a total NH_3 flow rate of 0.25 L/min.[16]

Catalyst Preparation. PVP-stabilized colloidal Au nanoparticles (SigmaAldrich, MW 29000, $[PVP]_{monomer}/[Au]$ = 10/1) were synthesized by adding an appropriate amount of a freshly prepared solution of $NaBH_4$ ($NaBH_4$/Au = 10/1) in 5 mL of methanol to a methanol solution (20 mL) containing PVP and $HAuCl_4 \cdot 3H_2O$. The resulting red solution was stirred for 16 h to ensure complete decomposition of $NaBH_4$,[37] since sodium borohydride can reduce oxygen-containing surface groups on carbon.[38,39] Next, colloidal nanoparticles were immobilized on supports by rapidly adding the colloid solution to the support suspended in a small volume of methanol with vigorous stirring. Methanol was used instead of typically employed water in order to avoid inhomogeneous deposition of Au nanoparticles. Alcohols have better interaction with both hydrophilic and hydrophobic carbon materials and can improve metal adsorption on hydrophobic carbons.[40,41] The amount of support material was adjusted to allow 1 wt % metal loading. Typically, adsorption of colloidal particles on the surface of the carbon material was achieved within 30 min, as evidenced by the disappearance of the red color of the solution. The obtained solid was recovered by centrifugation, washed several times with methanol and diethyl ether, and subsequently dried at 60 °C overnight. PVP was removed from supported Au nanoparticles by washing the catalyst in an excess of Milli-Q water at room temperature overnight.[42] Hence, no high-temperature treatments/reductions, which could have altered the surface properties of HSAG materials, have been employed. Gold nanoparticles supported on pristine HSAG are denoted as Au/HSAG and the rest as Au/HSAG-x, where x indicates the type of support treatment: ox, oxidation; H. reduction; N. amination.

Support and Catalyst Characterization. N_2 physisorption was performed at 77 K using a Micromeritics Tristar 3000 instrument. Prior to the measurement the samples were dried under N_2 flow at 200 °C for 20 h. Surface areas were calculated using the BET method, and the pore size distribution was calculated by analyzing the N_2 adsorption branch of isotherms using the BJH method. The BJH model was modified according to the Faas correction, and the empirical form of the Harkins−Jura equation was considered as a thickness reference curve. The total pore volume was calculated as a single point pore volume at a P/P_0 value of of 0.99. Acid−base titrations were performed using a TitraLab pH meter. HSAG samples (10−50 mg) were suspended in 65 mL of 0.1 M KCl solution. The suspension was degassed with N_2 flow for 5 min with vigorous stirring, and titrations were performed using either 0.01 M NaOH or 0.01 M HCl in 0.1 M KCl solutions. Concentrations of basic/acidic sites on HSAG materials were calculated from the equivalence point of titration curves. The points of zero charge (PZC) of HSAG supports were determined using the mass titration method.[43] HSAG materials (1, 2, 4, 6, 8, and 10 wt %) were suspended in 5 g of Milli-Q water, equilibrated for 24 h under N_2 bubbling; the pH of the solution was measured using a PHM220 MeterLab instrument . PZC values for other materials were measured using a single-point pH measurement: support materials were suspended in Milli-Q water (10−20 wt %), and the pH was measured after 24 h equilibration under N_2. X-ray photoelectron spectroscopy (XPS) was performed using a Thermo Scientific K-Alpha spectrometer equipped with a monochromated Al Kα ($h\nu$ = 1486.6 eV) X-ray source with a pass energy of 200 eV and resolution 1 eV for survey spectra and 50 and 0.1 eV, respectively, for high-resolution spectra. The peak binding energies were calibrated against the C 1s peak at 284.5 eV. Quantitative analysis of XPS data was performed using the Casa XPS program. The main C 1s peak of the sp^2 carbon in the high-resolution C 1s spectra was described using an asymmetric Doniach−Sunjic profile, while the rest of the peaks (N 1s, O 1s, and C 1s peaks of functional groups and shake-ups) were described with Gaussian−Lorentzian profiles after subtracting a Shirley background. Thermogravimetric analysis (TGA) was performed using a PerkinElmer Pyris 1TGA. Samples (5−10 mg) were heated in an Ar flow at a rate 5 °C/min up to 950 °C.

X-ray diffraction analysis (XRD) was performed using a Bruker-AXS D2 Phaser X-ray diffractometer with Co Kα radiation (λ = 1.79026 Å) operated at 30 kV and 10 mA. The average size of Au crystallites was estimated using the Scherrer equation with a shape factor k = 0.9 and line broadening

DOI: 10.1021/acscatal.7b00829
ACS Catal. 2017, 7, 4581−4591

analysis on the Au 111 peak. Transmission electron microscopy was performed on a Tecnai12 instrument operating at 120 eV. Catalyst powders were suspended in ethanol and deposited onto a carbon-coated Cu grid. Typically, at least 300 particles were counted to calculate the average particle diameter. Catalyst metal loadings were determined using inductively coupled plasma mass spectrometry (ICP-MS) performed on a ThermoFisher Scientific Element 2 instrument. Known amounts of Au/HSAG catalyst samples (10−20 mg) were loaded onto calcination boats and heated to 800 °C (10 °C/min heating rate) in static air to remove the carbon support. The remaining Au was dissolved with freshly prepared aqua regia. The obtained solution was transferred to a volumetric flask and diluted with Milli-Q water, and the Au concentration was measured using ICP-MS.

Catalyst Testing and Adsorption Experiments. Oxidation of HMF was performed in stainless steel autoclaves with a total volume of 12 mL. Typically, 25 mg of a catalyst was suspended in 7 mL of deionized water containing 0.2 mmol of HMF and 0.4 mmol of $NaHCO_3$. Reactors were heated to 90 °C and pressurized with 10 bar of O_2 with vigorous stirring (900 rpm). Samples of the reaction mixture were withdrawn, filtered with 0.2 μm PTFE filters, diluted with water, and analyzed using a Shimadzu LC-20AD high-performance liquid chromatograph equipped with a Bio-Rad Aminex HPX-87H column. Sulfuric acid (5 mM) at 333 K with a flow rate of 0.55 mL/min was used as an eluent. Each catalyst was tested at least twice to check reproducibility. Turnover frequencies (h^{-1}) were calculated as

$$\mathrm{TOF}\ (h^{-1}) = kC^0(\mathrm{HMF})/n_{\mathrm{Au\ surf}}$$

where k is the rate constant obtained from the fitting of the HMF conversion kinetic curves (first order kinetics), C^0 is the initial concentration of HMF, and n_{Au} is the total number of moles of surface gold.

For the study of the adsorption of HMF and HMFCA on Au/HSAG-x catalysts, 50 mg of a catalyst was suspended in 5 mL of an aqueous solution containing HMF/HMFCA (25 μmol) and $NaHCO_3$ (pH 8.5). The suspension was sonicated and further kept for 3 h without stirring. Next, Au/HSAG was filtered off and a 1 mL aliquot of the solution was mixed with 20 μL of 0.23 M dioxane (external standard) solution in water. The concentration of HMF in the obtained solutions was analyzed using high-performance liquid chromatography.

RESULTS

Modification of High-Surface-Area Graphite. The surface atomic compositions of pristine high-surface-area graphite (HSAG) as well as oxidized (HSAG-ox), reduced (HSAG-H), and aminated (HSAG-N) calculated from peak areas of the X-ray photoelectron survey spectra (Figure S1 in the Supporting Information) are summarized in Table 1. The pristine HSAG possesses a pronounced O 1s peak at 530 eV corresponding to the presence of 5.6% of surface oxygen in the form of oxygen-containing functional groups. An increase in the atomic surface concentration of oxygen from 5.6% to 12.6% was observed after a 5 min treatment of HSAG with hot HNO_3 vapor (HSAG-ox), confirming further introduction of oxygen-containing species. The surface atomic concentration of oxygen decreased to 3.3% after the thermal treatment in a H_2/N_2 flow at 400 °C (HSAG-H) due to the decomposition of thermally unstable O groups. Finally, upon treatment with gaseous ammonia (HSAG-N) nitrogen-containing surface species form at the expense of oxygen species; only 1.2 and 0.9% of oxygen and nitrogen, respectively, were detected on the surface of HSAG-N. The high temperature of the amination treatment explains why only a small number of the most thermally stable oxygen- and nitrogen-containing groups remain on the surface of HSAG-N.[14,44]

Table 1. Surface Elemental Composition of the Pristine, Oxidized, Reduced, and Ammonia-Treated HSAG Quantified from XP Survey Spectra

material	C, atom %	O, atom %	N, atom %	O/C	N/C
HSAG	94.4	5.6		0.059	
HSAG-ox	87.0	12.6	0.4	0.145	0.005
HSAG-H	96.7	3.3		0.034	
HSAG-N	97.8	1.3	0.9	0.013	0.009

The nature and relative amounts of the surface functional groups were established by analyzing high-resolution spectra of C 1s and N 1s bands (Figure 2 and Table 2). It is generally accepted that the C 1s peak in oxygen-containing carbons can be deconvoluted with the following components: peak at 284.5−284.6 eV due to sp^2-hybridized carbon, peak at 286.1−286.3 eV due to carbon bound to oxygen with a single bond (C−O, ethers and phenols), peak at 287.4−287.7 eV due to carbonyl groups (C═O, quinones and ketones), peak at 288.6−290.0 eV due to carbon bound to two oxygens (O═C−O, carboxyls, lactones, and esters), and shakeup satellites of carbon in aromatic systems at 290.5 and 292 eV.[18,44,45]

When both oxygen- and nitrogen-containing functionalities are present on the surface of the carbon material, the contributions from C−N and C−O overlap in the region 285−290 eV, making C 1s spectra extremely complex; therefore, no deconvolution of the C 1s spectrum of HSAG-N was performed. Figure 2 and Table 2 show that functional groups comprising a C−O bond are dominant among the oxygen-containing groups on the surface of the pristine HSAG. After thermal treatment under H_2/N_2 flow concentrations of all oxygen-containing surface species had decreased due to thermal decomposition.[14] After HSAG oxidation with HNO_3 the vapor relative concentration of COO− groups increased from 3.8 to 6.1%, indicating the incorporation of a large number of carboxyl, lactone, and ester groups. The relative concentration of C−O groups increased from 5.8 to 6.7%, while the concentration of C═O groups showed a slight decrease from 3.2 to 2.6%, which could be due to the partial conversion of the C═O groups into COO− groups upon HNO_3 treatment.

Deconvolution of the high-resolution N 1s spectrum of HSAG-N (Figure S2 in the Supporting Information) showed that N-containing species consisted primarily of pyridinic groups. Other groups included quaternary, pyrrolic, and N-oxide species. Thus, XPS characterization shows that a range of HSAG materials with distinctly different oxygen contents and natures of functional groups had been prepared.

Information about the amount of thermally removable groups of HSAG materials was obtained from thermogravimetric analysis (TGA, Figure S3 in the Supporting Information). HSAG-ox showed the highest (ca. 12%) overall weight loss upon heating within the temperature range 200−950 °C under an inert atmosphere, while HSAG, HSAG-H, and HSAG-N demonstrated lower weight loss values of 10, 6, and 3.7 wt %, respectively. The trend in the weight loss qualitatively agrees with the HSAG-x oxygen content determined from XPS.

DOI: 10.1021/acscatal.7b00829
ACS Catal. 2017, 7, 4581−4591

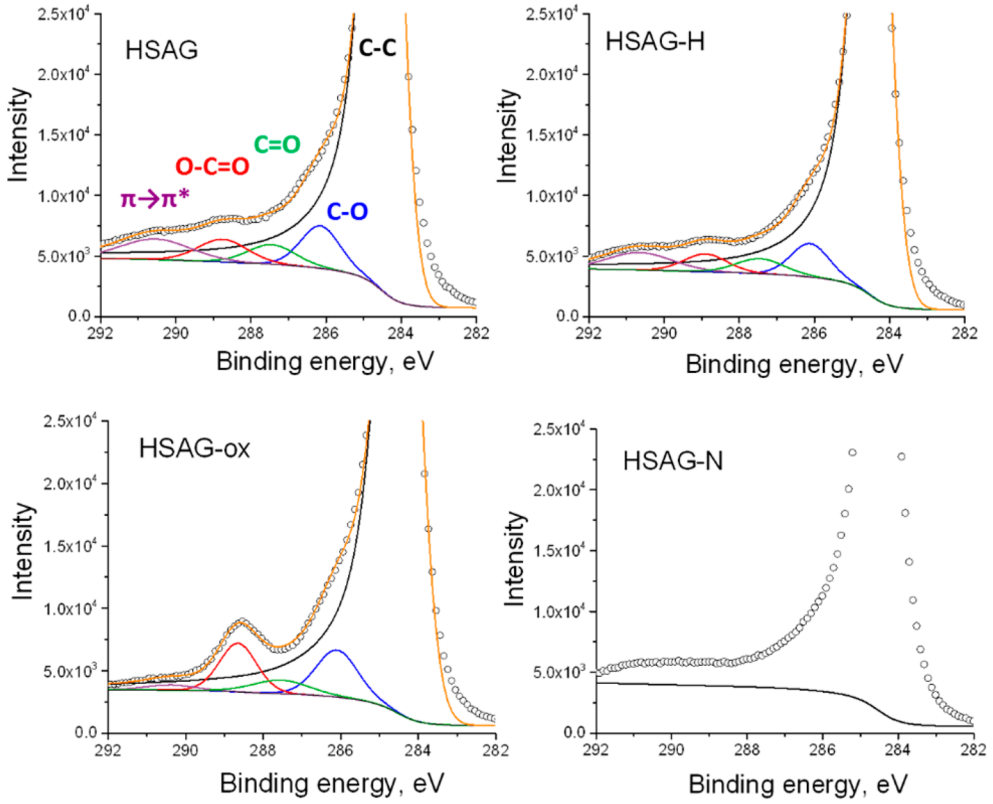

Figure 2. High-resolution C 1s XP spectra of the pristine, oxidized, reduced, and ammonia-treated HSAG. A Shirley background is applied to remove the contribution of the inelastically scattered electrons. Color scheme: blue, surface groups comprising C−O; green, C═O; red, O═C−O; black, sp^2 carbon; purple, shakeup satellites; orange, overall fitting.

Table 2. Relative Percentage of Functional Groups in Pristine, Oxidized, and Reduced HSAG Derived from C 1s XP Spectra

	C−C, %	C−O, %	C═O, %	O═C−O, %	$\pi \rightarrow \pi^*$, %
HSAG	82.3	5.8	3.2	3.8	4.9
HSAG-H	83.9	5.3	2.9	3.2	4.7
HSAG-ox	83.7	6.7	2.6	6.1	0.9

The acid−base properties of HSAG materials were studied by determining their points of zero charge (PZC) and concentrations of acid/base sites. The results of the PZC determination of HSAG materials using the mass titration method (Figure 3A and Table 3) show that the acidity of HSAG materials correlates with the oxygen content: the PZC

Table 3. Properties of the Untreated and Treated HSAG

material	S_{BET}, m^2/g	V_{pore}, mL/g	d_{pore}, nm	acidic sites, nm^{-2}	basic sites, nm^{-2}	PZC
HSAG	502	0.78	5.4	0.16		4.0
HSAG-ox	443	0.64	5.8	0.54		2.6
HSAG-H	507	0.69	5.4		0.03	7.7
HSAG-N	506	0.70	5.5		0.09	9.9

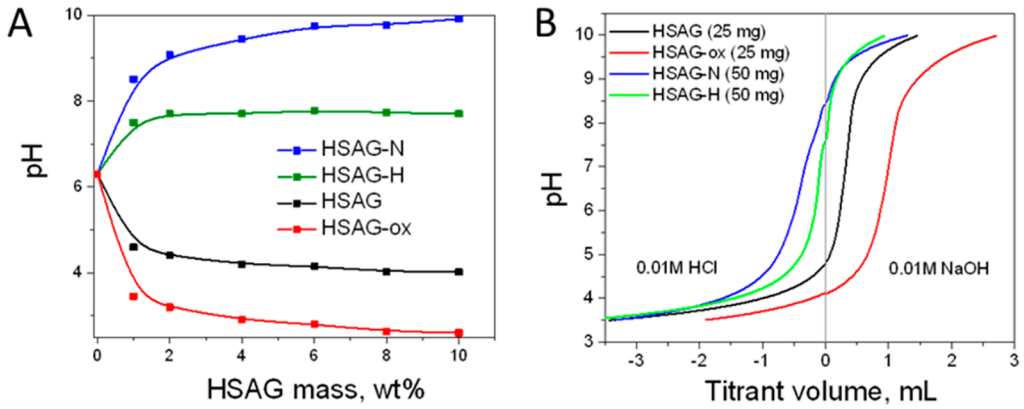

Figure 3. (A) Mass titration of HSAG-x in Milli-q H_2O (solid lines are given as a guide for the eye). (B) Acid/base titration with 0.01 M NaOH and 0.01 M HCl of pristine, reduced, oxidized, and aminated HSAG in 65 mL of KCl solution.

DOI: 10.1021/acscatal.7b00829
ACS Catal. 2017, 7, 4581−4591

of HSAG-x materials increases in the order HSAG-ox < HSAG < HSAG-H < HSAG-N. The pristine HSAG is acidic with a PZC value of 4.0. The acidity of the pristine HSAG originates from the surface groups, such as carboxyls, phenols, and lactones, located on the inner pore walls of HSAG as determined from the XPS data. HSAG-ox is more acidic with a PZC value of 2.6 due to strongly acidic functional groups introduced by the HNO_3 treatment. HSAG-H is mildly basic with a PZC value of 7.7. Since acidic oxygen-containing groups (carboxylic, lactone) are thermally less stable than basic groups (quinone, pyrone, chromene), they decompose preferentially at lower temperature under a reducing atmosphere, thus increasing the surface basicity.[14] HSAG-N demonstrates the highest basicity of this series with a PZC value of 9.9. The basicity of HSAG-N originates from pyridinic and pyrrolic groups as well as delocalized π electrons of the graphene sheets.[16,46] These results show that the PZC of HSAG can be varied within a broad range (2.6−9.9) by surface functionalization.

The concentrations of acidic and basic groups on HSAG surfaces were established using acid/base titration. The initial pH values of the titration curves (Figure 3B) also showed that HSAG and HSAG-ox were acidic, while HSAG-H and HSAG-N were (mildly) basic. The apparent concentrations of surface acidic and basic sites of HSAG materials are given in Table 3.

N_2 physisorption results (Table 3) show that there were no major changes in the surface area, pore size, or pore volume of HSAG during the employed treatments. A small decrease in the surface area and pore volume of HSAG-ox in comparison to those of the pristine HSAG can be attributed to the textural damage during the oxidation treatment. Graphitic carbon materials free of surface functional groups are hydrophobic.[41] It is well-known that the presence of polar surface groups, e.g. oxygen- or nitrogen-containing groups, increases carbon hydrophilicity. Therefore, the hydrophilicity of HSAG materials is expected to decrease in the order HSAG-ox > HSAG > HSAG-H ≈ HSAG-N.

In summary, a range of HSAG materials with similar morphologies but different surface properties, i.e. surface elemental composition, nature and concentration of functional groups, and acid−base and hydrophilic properties, have been prepared. These materials were used as supports to deposit gold colloids.

Au Deposition on HSAG-x. Figure 4 shows representative TEM micrographs of Au/HSAG-x catalysts and the corresponding particle size distribution histograms. The size of the gold colloid before immobilization was 2.3 ± 0.8 nm (Figure S4 in the Supporting Information). The results show that spherical gold nanoparticles with sizes of 2−4 nm are uniformly distributed over the surface of the HSAG supports. The size of the supported Au particles is slightly larger than that of the original gold colloids, especially when the particles are immobilized on HSAG materials with higher oxygen content. For the most basic material HSAG-N with the lowest oxygen content the size and size distribution of gold particles did not change upon deposition. These results indicate that basic carbon materials can better stabilize the size of supported particles deposited from colloidal solution, which is in agreement with previous reports.[25] Results of XRD analysis (Table 4) agreed well with the results of the TEM study, and no large Au crystallites were detected. Au loadings were close to the target value of 1 wt % in all cases.

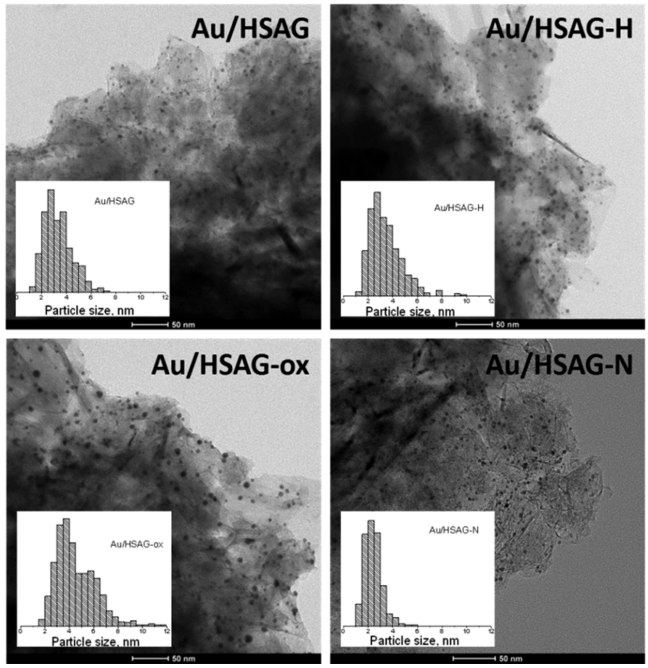

Figure 4. Representative TEM micrographs and corresponding particle size distribution histograms of Au/HSAG, Au/HSAG-H, Au/HAS-ox, and Au/HSAG-N.

Table 4. Gold Particle (TEM) and Crystallite (XRD) Sizes and Loadings (ICP-MS) of Au/HSAG-x Catalysts

support	particle size,[a] nm	crystallite size, nm	Au loading, wt %
HSAG	3.3 ± 1.1	3.7	1.0
HSAG-H	3.4 ± 1.3	3.7	1.2
HSAG-ox	4.6 ± 1.3	4.3	1.2
HSAG-N	2.4 ± 0.7	3.2	1.1

[a]Number-average value.

Oxidation of 5-Hydroxymethylfurfural. We first investigated the activity of Au-free HSAG supports in the oxidation of HMF using $NaHCO_3$ as a base. It was recently reported that metal-free nitrogen-doped carbon materials can demonstrate some activity in the aerobic oxidation of alcohols.[47] Our results show that the concentration of HMF in the reaction mixture decreased by up to ca. 15% in 12 h; however, no HMFCA, FDCA, or any other products formed. This decrease in the concentration is due to HMF adsorption onto the porous HSAG-x (see below). The 15% decrease in HMF concentration corresponds to a surface coverage of ~1.4 HMF molecule/nm^2 of HSAG. Therefore, we concluded that metal-free HSAG supports are inactive in HMF oxidation but strongly adsorb it.

Au/HSAG-x catalysts were active in the oxidation of HMF under mildly basic conditions (pH 8−8.5, $NaHCO_3$ base). HMFCA is the main intermediate, and DFF does not form in the presence of gold catalysts, while FFCA is quickly converted into FDCA and therefore its concentration is close to zero during the reaction, in line with previous reports.[6,12,26,48,49] No activity was observed when $NaHCO_3$ was not added to the reaction.

Figure 5 shows reaction profiles of HMF oxidation in the presence of Au/HSAG-x. Conversion of HMF is well described by first-order kinetics. Gold nanoparticles supported on basic carbon materials were more active in both conversion of HMF into HMFCA and further conversion of HMFCA to FDCA in

DOI: 10.1021/acscatal.7b00829
ACS Catal. 2017, 7, 4581−4591

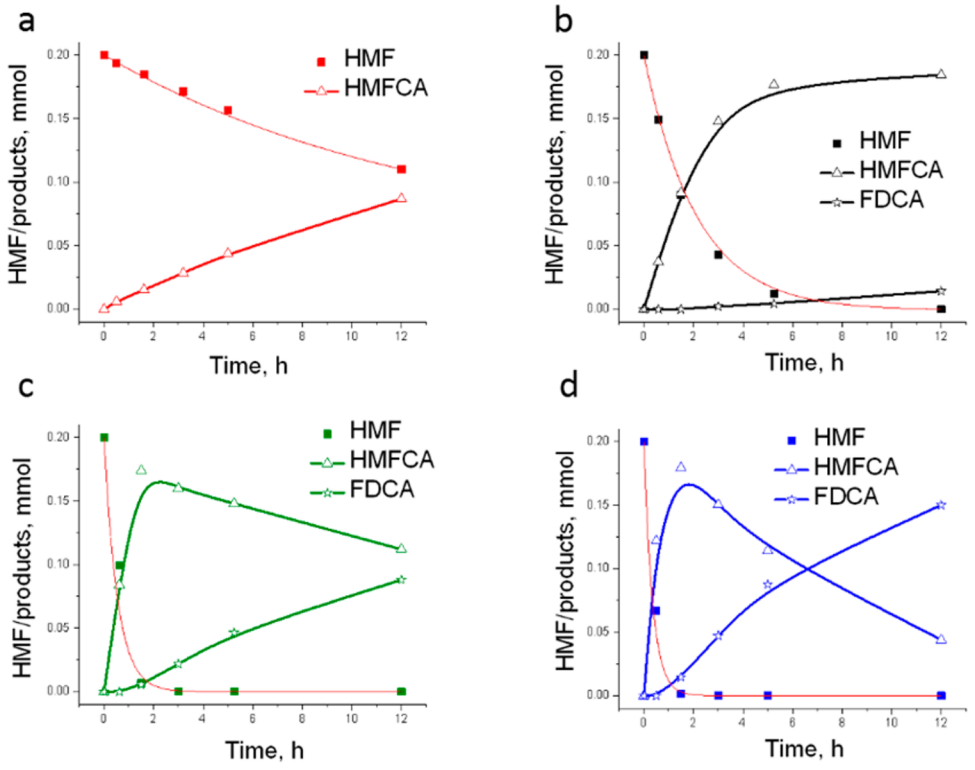

Figure 5. Reaction profiles of HMF oxidation in the presence of (a) Au/HSAG-ox, (b) Au/HSAG, (c) Au/HSAG-H, and (d) Au/HSAG-N. Conditions: HMF 0.2 mmol, [HMF]/[Au] = 160, $NaHCO_3$ 0.4 mmol, H_2O 7 mL, O_2 10 bar, 90 °C, 900 rpm. Solid red lines in HMF conversion profiles are first-order kinetic fits, while solid lines in product profiles are provided to guide the eye.

Table 5. Oxidation of HMF in the Presence of Au/HSAG-x Catalysts[a]

catalyst	support PZC	HMF conversion,[b] %	$TOF_{Au\ surf}$,[c] h^{-1} (HMF conversion)	FDCA max formation rate/Au_{surf},[d] h^{-1}	yield of HMFCA,[b] %	yield of FDCA,[b] %
Au/HSAG-ox	2.6	45	25		43	0
Au/HSAG	4.0	>99	273	4	93	6
Au/HSAG-H	7.7	>99	969	28	56	44
Au/HSAG-N	9.9	>99	1195	46	22	75

[a]Conditions: HMF 0.2 mmol, [HMF]/[Au] = 160, $NaHCO_3$ 0.4 mmol, H_2O 7 mL, O_2 10 bar, 90 °C, 900 rpm. [b]Conversion and product yields are calculated after 12 h. [c]TOF values are calculated as initial reaction rate divided by the number of moles of surface Au on the basis of the initial particle size. [d]Maximum FDCA formation rate calculated from the steepest region in FDCA formation curves and normalized to surface Au on the basis of the particle size after 30 min.

comparison to the catalysts supported on acidic carbons. In the presence of Au/HSAG-ox the reaction did not reach full HMF conversion and no FDCA was detected even after 40 h. Gold nanoparticles supported on acidic HSAG were most selective toward HMFCA formation (>90% selectivity). Although the initial gold particle sizes differ slightly within the Au/HSAG series, differences in activity cannot be explained by the difference in the specific gold surface area. TOF values normalized to the surface Au for HMF conversion and the normalized rate of FDCA formation are shown in Table 5. The highest TOF value of ca. 1195 h^{-1} was achieved for Au/HSAG-N, while the lowest TOF value of 25 h^{-1} was observed for Au/HSAG-ox. The catalyst activity clearly increases with the PZC value of the support (Figure S5 in the Supporting Information). Therefore, we conclude that the observed differences are due to the different surface properties of HSAG-x supports.

Au Particle Stability. Details on the Au particle/crystallite sizes before and after HMF oxidation are given in Table 6. We observed growth of 2−4 nm Au particles into larger monocrystalline particles during HMF oxidation on all four

Table 6. Au Crystallite Sizes before, during, and after HMF Oxidation (12 h)

		Au crystallite size, nm		
catalyst	O, atom %	initial	after 30 min in HMF oxidation	after reaction (12 h)
Au/HSAG-ox	12.6	4.3	5.1	10.3
Au/HSAG	5.6	3.7	4.0	10.0
Au/HSAG-H	3.3	3.7	4.0	7.3
Au/HSAG-N	1.3	3.2	3.2	5.9
Au/HSAG-N[a]	1.3	3.2	-	5.9

HSAG supports. Particles grew less on more basic HSAG. The Au crystallite growth was irrespective of whether HMF was added or not (Table 6). Hence, particle growth is not induced by the catalytic process itself but rather by the exposure to the reaction conditions involving high temperatures and aqueous media at basic pH.

Growth of metal nanoparticles can occur via two main mechanisms. First, particles can diffuse over the surface as a

DOI: 10.1021/acscatal.7b00829
ACS Catal. 2017, 7, 4581−4591

Scheme 2. Overall Mechanism of HMF Oxidation to FDCA Adapted from Davis et al.[12]

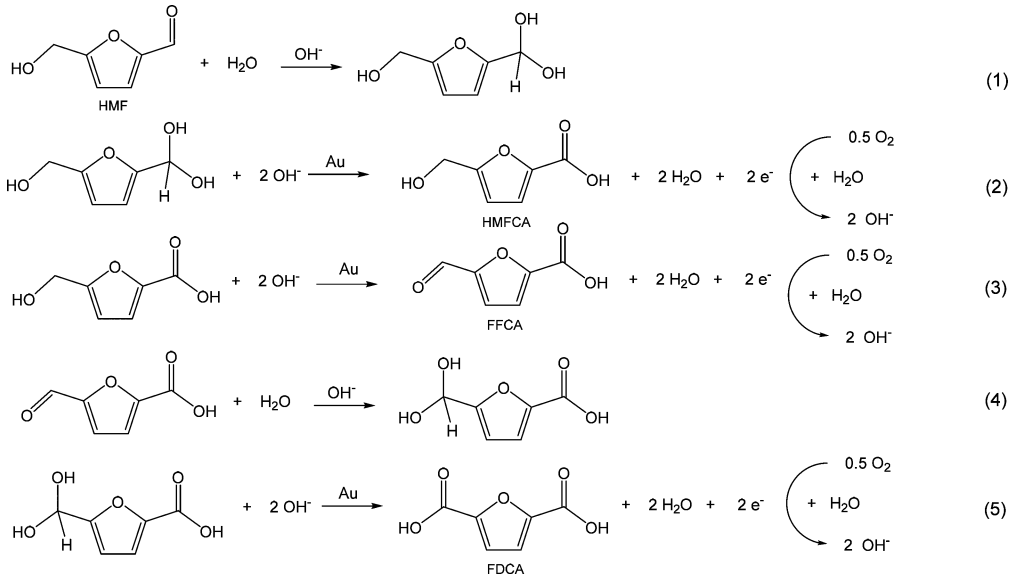

whole and coalesce with other particles. Second, metal particles can release coordinated metal species which diffuse and add to the larger particles (Ostwald ripening).[50,51] From Table 6 it is clear that the presence of oxygen-containing groups on the surface of carbon support facilitates Au particle growth. It is was previously observed that surface oxygen groups can assist Au particle growth.[52] The presence of oxygen groups near gold nanoparticles can decrease the degree of adhesion of Au nanoparticles to the support[53] and thus allow for better mobility of Au nanoparticles.[54] Alternatively, oxygen surface groups can facilitate the formation and movement of oxidized mobile Au species. The investigation of the exact mechanism of the growth of Au nanoparticles under oxidative conditions in the liquid phase is beyond the scope of this work and is the topic of an ongoing investigation. However, we can conclude that the poor Au particle stability in aqueous-phase HMF oxidation can be related to oxygen-containing groups on the carbon support surface.

DISCUSSION

Origin of Different Activity/Selectivity of Au/HSAG-x. Here Au/HSAG-x catalysts were investigated in HMF oxidation in the presence of $NaHCO_3$. The highest achieved TOF value of HMF conversion was 1195 h^{-1} for Au/HSAG-N, which is ca. 7−15 times lower than the values reported previously for carbon-supported gold catalysts.[6,11] This is because a milder base ($NaHCO_3$) was used in this work as opposed to the NaOH typically used for HMF oxidation. Strongly alkaline conditions were previously shown to be undesirable for HMF oxidation because of the poor stability of HMF at high pH. Besson et al. demonstrated that HMF rapidly degraded to 2,5-bis(hydroxymethyl)furan (BHMF) and levulinic and formic acids as well as insoluble humins in the presence of NaOH (pH 13) and Na_2CO_3 (pH 11.5) at 100 °C and 40 bar of air, while no HMF degradation was observed in the presence of the mild base $NaHCO_3$.[9] Davis et al. observed the formation of up to 13% of BHMF byproduct, induced by high concentration of the NaOH base, while no BHMF byproduct was observed in our study, most likely due to the mild pH. Comparison of Au/HSAG-N with Pt/C in the presence of $NaHCO_3$ base (100 °C, 40 bar of air, HMF/Pt = 100, $NaHCO_3$/HMF = 4)[55] shows that Au/HSAG-H is ca. 5 times more active in HMF oxidation than carbon-supported Pt catalyst, despite the milder conditions used for HMF oxidation in the presence of Au/HSAG-N. These results indicate that Au catalysts supported on basic carbon materials are promising catalysts for highly selective HMF oxidation to FDCA under mildly basic conditions.

The mechanism of HMF oxidation over supported gold catalysts in basic aqueous media was investigated by Davis et al. (Scheme 2).[12] As seen from Scheme 2, hydroxyls play an important role in HMF oxidation. OH^- ions catalyze the formation of geminal diols from aldehyde and water (Scheme 2, steps 1 and 4). Furthermore, OH^- ions adsorbed on the gold surface or at the gold−support interface abstract hydrogen from C−H and O−H groups of alcohol or geminal diol to yield carbonyl and carboxylic groups, respectively (Scheme 2, steps 2, 3, and 5).[10] While the formation of geminal diols can be catalyzed by OH^- in solution, dehydrogenation steps are catalyzed by hydroxyls adsorbed on the surface (or in the close vicinity) of gold, since electron density formed as a result of hydrogen abstraction present on the gold nanoparticles. The electrons are then scavenged by oxygen to regenerate the hydroxyls (Scheme 2, steps 2, 3, and 5, right side).

In this work HMF oxidation was performed under mildly basic conditions. The pH of the reaction mixture was 8.0−8.5 before the catalytic reaction start and 7.5−8.0 after 12 h. The drop in pH is due to base neutralization with the formed HMFCA and FDCA acids.

When the pH of solution is lower than the PZC value of a suspended solid, surface groups become protonated and therefore the surface of the material is positively charged.[56] If pH of the solution is higher than the PZC value, a part of the surface groups becomes deprotonated and the surface is negatively charged. Therefore, the surface of HSAG and HSAG-ox (PZC 2.6−4.0) was negatively charged during the reaction, while the surface of basic materials, HSAG-H and HSAG-N (PZC 7.7−9.9), was either neutral or slightly positively charged.

On the basis of the proposed reaction mechanism and catalyst characterization results, we can tentatively give the

DOI: 10.1021/acscatal.7b00829
ACS Catal. 2017, 7, 4581−4591

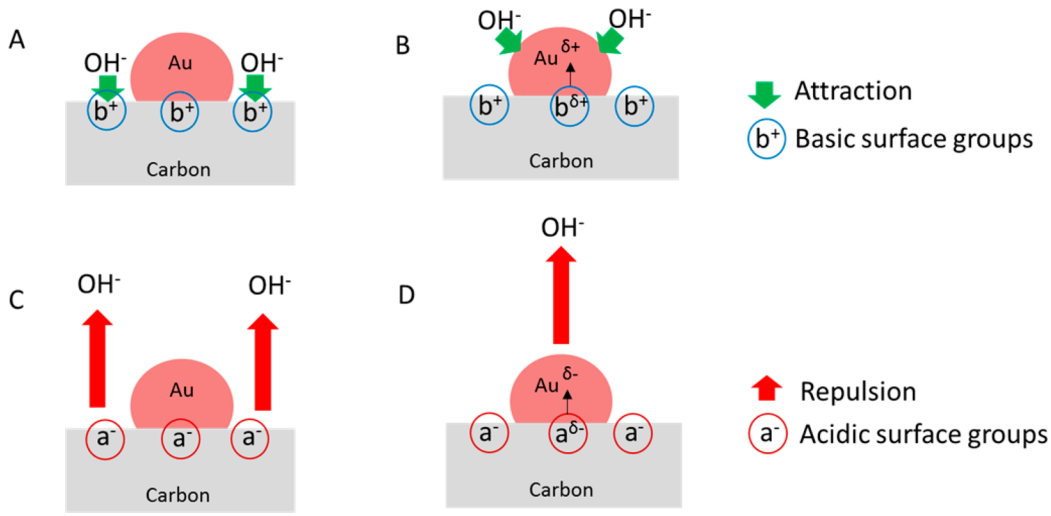

Figure 6. Two possible scenarios of how acidic or basic surface groups on the carbon support can affect the adsorption of OH^-. Hydroxyls adsorbed on gold nanoparticles or at the gold−support interface are necessary for efficient hydrogen abstraction in steps 2, 3, and 5 in Scheme 2. Acidic or basic groups can affect adsorption of OH^- on the support near the metal−support interface (A, C) or transfer charge to gold nanoparticles, which affects adsorption of ions on the gold (B, D).

following explanations of the observed differences between acidic and basic Au/HSAG-x catalysts.

First, acidic HSAGs are highly hydrophilic. As was previously suggested by Besson et al.,[28] higher hydrophilicity of the support material results in a stronger adsorption of water molecules on the support surface, which compete for the adsorption sites with the HMF substrate and HMFCA intermediate. Table S1 in the Supporting Information shows HMF and HMFCA adsorption on Au/HSAG-x and pure HSAG-x supports. The lowest adsorption of both HMF and HMFCA is observed for the most acidic support HSAG-ox and Au/HSAG-ox. However, the difference in the adsorption values of HMF is not significant enough to explain the 50-fold difference in the activity within the Au/HSAG-x series.

A second possible reason is the different stabilities of Au nanoparticles on acidic and basic HSAG. The lower stability of gold nanoparticles on acidic HSAG supports results in a faster decrease in the active Au surface area. Since Au particles grow to larger sizes on acidic HSAG, we calculated TOF values considering the final size of gold nanoparticles in order to find out if the observed lower activity of the acidic catalysts could be solely related to the more pronounced particle growth (Table S2 in the Supporting Information). The results show that, even assuming that particles grow instantaneously to the final size, the most basic Au/HSAG-N is still ca. 37 times more active than Au/HSAG-ox. From Table 6 it is clear that particles do not grow instantaneously. This result suggests that the stability difference of gold nanoparticles on different supports is not the reason for the observed differences in activity.

This means that the difference in activity must be mainly related to the charge of carbon supports with acidic and basic groups. There are two possible ways in which surface charge of carbon supports could affect the activity of gold nanoparticle catalysts in HMF oxidation. The positively charged surface of basic carbons facilitates adsorption of OH^- ions onto the surface of the catalyst support in the close vicinity of gold nanoparticles: i.e., at the gold−support interface (Figure 6A). Since gold catalyzes dehydrogenation (Scheme 2) only in the presence of adsorbed OH^-, more adsorption of OH^- and therefore a higher local concentration of OH^- in the near vicinity of gold for basic carbons result in an increase in the rates of dehydrogenation to yield HMFCA, FFCA, and FDCA (Scheme 2, steps 2, 3, and 5). Negatively charged groups on the surface of acidic carbons repel OH^- ions, which results in a reduction of the rates of the hydrogen abstraction steps (Figure 6C). This scenario is valid and causes considerable difference between the activities of acidic/basic supports for the active sites located at the periphery of gold nanoparticles (metal−support interface).

In the second scenario, surface charge can be transferred from the carbon support to gold nanoparticles, making them fractionally charged either positively in the case of basic surface groups (Figure 6B) or negatively in the case of supports with acidic surface groups (Figure 6D). The positively charged Au nanoparticles attract OH^- ions, which results in an increase in dehydrogenation activity. This case is valid for all Au active sites and not necessarily sites located close to the metal−support interface. The two scenarios described above are not mutually exclusive: i.e., both can be realized at the same time. Detecting a fractional charge change induced by the support for 3 nm gold nanoparticles is difficult, because support surface charge is generated in situ depending on the pH of the solution; therefore, special in situ catalyst characterization would be required. Moreover, the charge induced in the 3 nm gold nanoparticles is shared among ∼800−900 constituent Au atoms and is therefore difficult to detect, yet it might have a non-negligible effect on the catalyst activity.

The high selectivity toward HMFCA for catalysts supported on acidic HSAG is likely due to the deprotonated (anionic) form of HMFCA under the reaction conditions (the pK_a value of HMFCA is 3.1, reaction pH >7.5). Therefore, HMFCA anions are repelled by the negatively charged groups (0.16−0.54 nm^{-1}) of acidic HSAG supports or negative charge on gold nanoparticles, preventing their further oxidation to FDCA. On the other hand, the positively charged surface of basic carbons or positive charge of gold nanoparticles facilitate adsorption of HMFCA anions on/to the vicinity of gold nanoparticles, thus promoting their further conversion. This explanation is supported by the fact that HMFCA is adsorbed >6 times less on Au/HSAG-ox than on Au/HSAG-N (Table S1

DOI: 10.1021/acscatal.7b00829
ACS Catal. 2017, 7, 4581−4591

in the Supporting Information), which can be due to the difference in electrostatic interaction. Therefore, Au catalysts supported on acidic oxidized carbon supports can be used for highly selective synthesis of HMFCA from HMF.

The improved adsorption of HMFCA and hydroxyl anions might also explain the high FDCA yield for the basic Au/CNF-N observed in the work by Davis et al.[11] Wang et al. observed that the presence of carbonyl/quinone groups on carbon nanotubes (CNT) supports improved the yield of FDCA, while carboxylic groups on CNT were detrimental.[26] Quinone groups are known to be basic, and carbonyl groups are often constituents of other types of basic functional groups (e.g., pyrone), explaining the improved adsorption of HMF and intermediates observed in the work. On the other hand, the acidic and more hydrophilic nature of carboxylic groups accounts for the reduced adsorption/activity for the catalysts with surfaces rich in carboxylic groups.

CONCLUSIONS

A relationship between the surface properties of carbon supports and the performance of gold nanoparticles supported on these carbon materials in the oxidation of HMF under mildly basic conditions has been established. The activity of Au/HSAG-x in HMF oxidation and the selectivity toward FDCA increase with support basicity, reaching a TOF value of 1195 h^{-1} for HMF conversion for the most basic catalyst support. In contrast, gold nanoparticles supported on acidic carbons with a high density (up to 0.54 nm^2) of oxygen functional groups showed much lower activities (25 h^{-1} for the most acidic) and a high selectivity (>90%) toward the intermediate monoacid HMFCA. The stability of the supported gold nanoparticles is affected by the surface chemical composition: particles supported on basic carbons with low densities of surface functional groups show good stability, while oxygen-containing surface groups facilitate particle growth.

The differences in catalytic activity and selectivity between gold nanoparticles supported on acidic and basic carbon supports are proposed to be mainly due to the differences in the adsorption of hydroxyls and charged reaction intermediates. Hydroxyl anions adsorbed on gold nanoparticles or at the metal−support interface are essential for hydrogen abstraction from alcohol and geminal diol groups, leading to the formation of carbonyl and carboxylic groups, respectively. We propose that surface groups of basic carbon supports (HSAG-H and HSAG-N), which are charged positively under the reaction conditions, either facilitate efficient adsorption of hydroxyls OH^- at the gold−support interface or induce (fractional) positive charge in gold nanoparticles, which leads to more efficient adsorption of hydroxyls on the Au surface. For acidic carbon supports the opposite scenario is true: hydroxyl anions are repelled from the negatively charged support surface or gold nanoparticles, which leads to a reduction in dehydrogenation rates. Positively charged surface groups also facilitate adsorption of the deprotonated intermediate monoacid HMFCA at the gold−support interface or gold surface, promoting its further conversion and thus increasing the yield of FDCA. In contrast, the negatively charged surface of acidic carbons HSAG and HSAG-ox or gold particles repel HMFCA anions, which results in high selectivity toward HMFCA.

These findings set design rules for gold catalysts that are highly active in HMF oxidation and selective toward FDCA: one should use supports that are positively charged under the reaction conditions. In contrast, to obtain catalysts that are highly selective toward the intermediate monoacid HMFCA, supports that are negatively charged under the reaction conditions with a high density of surface functional groups should be employed.

ASSOCIATED CONTENT

Supporting Information

The Supporting Information is available free of charge on the ACS Publications website at DOI: 10.1021/acscatal.7b00829.

Additional XPS and TGA characterization data of carbon supports, TEM of the gold colloid, correlation of TOFs with the point of zero charge of the support, HMF and HMFCA adsorption on Au catalysts and bare supports, and TOF values calculated on the basis of the final Au particle size (PDF)

AUTHOR INFORMATION

Corresponding Authors

*B.D.: e-mail, B.Donoeva@uu.nl; tel, +31 30 253 7400.
*P.E.d.J.: e-mail, P.E.deJongh@uu.nl; tel, +31 30 253 17 47.

ORCID

Baira Donoeva: 0000-0002-1702-8857
Petra E. de Jongh: 0000-0002-2216-2620

Notes

The authors declare no competing financial interest.

ACKNOWLEDGMENTS

B.D. thanks the European Commission for funding from the European Union's Horizon 2020 research and innovation program under the Marie Skłodowska-Curie grant agreement No 703861; P.E.d.J. and N.M. gratefully acknowledge NWO Vici (N. 16.130.344). We thank Dr. Daniil Ovoshchnikov (group of Prof. Emiel Hensen, TU Eindhoven) for the acquisition of the XPS spectra, Marjan Versluijs for gravimetric analysis, Lisette Pompe, Thomas Hartmann, and Nynke Krans for TEM imaging, Peter Bramwell for N_2 physisorption analysis, and Pascal Wijten for the HPLC training.

REFERENCES

(1) Delidovich, I.; Hausoul, P. J. C.; Deng, L.; Pfützenreuter, R.; Rose, M.; Palkovits, R. *Chem. Rev.* **2016**, *116*, 1540−1599.
(2) Sheldon, R. A. *Green Chem.* **2014**, *16*, 950−963.
(3) Zhang, Z.; Deng, K. *ACS Catal.* **2015**, *5*, 6529−6544.
(4) Casanova, O.; Iborra, S.; Corma, A. *J. Catal.* **2009**, *265*, 109−116.
(5) Taarning, E.; Nielsen, I. S.; Egeblad, K.; Madsen, R.; Christensen, C. H. *ChemSusChem* **2008**, *1*, 75−78.
(6) Davis, S. E.; Houk, L. R.; Tamargo, E. C.; Datye, A. K.; Davis, R. J. *Catal. Today* **2011**, *160*, 55−60.
(7) Yi, G.; Teong, S. P.; Zhang, Y. *Green Chem.* **2016**, *18*, 979−983.
(8) Villa, A.; Schiavoni, M.; Campisi, S.; Veith, G. M.; Prati, L. *ChemSusChem* **2013**, *6*, 609−612.
(9) Ait Rass, H.; Essayem, N.; Besson, M. *ChemSusChem* **2015**, *8*, 1206−1217.
(10) Zope, B. N.; Hibbitts, D. D.; Neurock, M.; Davis, R. J. *Science* **2010**, *330*, 74−78.
(11) Davis, S. E.; Benavidez, A. D.; Gosselink, R. W.; Bitter, J. H.; de Jong, K. P.; Datye, A. K.; Davis, R. J. *J. Mol. Catal. A: Chem.* **2014**, *388−389*, 123−132.
(12) Davis, S. E.; Zope, B. N.; Davis, R. J. *Green Chem.* **2012**, *14*, 143−147.
(13) Ide, M. S.; Davis, R. J. *Acc. Chem. Res.* **2014**, *47*, 825−833.
(14) Figueiredo, J. L. *J. Mater. Chem. A* **2013**, *1*, 9351−9364.
(15) Bandosz, T. J. In *Carbon Materials for Catalysis*; Serp, P., Figueiredo, J. L., Eds.; Wiley: Hoboken, NJ, 2009; p 45.

DOI: 10.1021/acscatal.7b00829
ACS Catal. 2017, 7, 4581−4591

(16) Arrigo, R.; Hävecker, M.; Wrabetz, S.; Blume, R.; Lerch, M.; McGregor, J.; Parrott, E. P. J.; Zeitler, J. A.; Gladden, L. F.; Knop-Gericke, A.; Schlögl, R.; Su, D. S. *J. Am. Chem. Soc.* **2010**, *132*, 9616−9630.
(17) Xia, W.; Jin, C.; Kundu, S.; Muhler, M. *Carbon* **2009**, *47*, 919−922.
(18) Shafeeyan, M. S.; Daud, W. M. A. W.; Houshmand, A.; Shamiri, A. *J. Anal. Appl. Pyrolysis* **2010**, *89*, 143−151.
(19) Goncalves, G.; Marques, P. A. A. P.; Granadeiro, C. M.; Nogueira, H. I. S.; Singh, M. K.; Grácio, J. *Chem. Mater.* **2009**, *21*, 4796−4802.
(20) Villa, A.; Schiavoni, M.; Prati, L. *Catal. Sci. Technol.* **2012**, *2*, 673−682.
(21) Comotti, M.; Weidenthaler, C.; Li, W.-C.; Schüth, F. *Top. Catal.* **2007**, *44*, 275−284.
(22) Schüth, F. *Phys. Status Solidi B* **2013**, *250*, 1142−1151.
(23) Rodrigues, E. G.; Pereira, M. F. R.; Chen, X.; Delgado, J. J.; Órfão, J. J. M. *J. Catal.* **2011**, *281*, 119−127.
(24) Rodrigues, E. G.; Delgado, J. J.; Chen, X.; Pereira, M. F. R.; Órfão, J. J. M. *Ind. Eng. Chem. Res.* **2012**, *51*, 15884−15894.
(25) Prati, L.; Villa, A.; Chan-Thaw, C. E.; Arrigo, R.; Wang, D.; Su, D. S. *Faraday Discuss.* **2011**, *152*, 353−365.
(26) Wan, X.; Zhou, C.; Chen, J.; Deng, W.; Zhang, Q.; Yang, Y.; Wang, Y. *ACS Catal.* **2014**, *4*, 2175−2185.
(27) Zhou, C.; Deng, W.; Wan, X.; Zhang, Q.; Yang, Y.; Wang, Y. *ChemCatChem* **2015**, *7*, 2853−2863.
(28) Kerdi, F.; Ait Rass, H.; Pinel, C.; Besson, M.; Peru, G.; Leger, B.; Rio, S.; Monflier, E.; Ponchel, A. *Appl. Catal., A* **2015**, *506*, 206−219.
(29) Gong, J. *Chem. Rev.* **2012**, *112*, 2987−3054.
(30) Valden, M.; Lai, X.; Goodman, D. W. *Science* **1998**, *281*, 1647−1650.
(31) Miedziak, P. J.; Alshammari, H.; Kondrat, S. A.; Clarke, T. J.; Davies, T. E.; Morad, M.; Morgan, D. J.; Willock, D. J.; Knight, D. W.; Taylor, S. H.; Hutchings, G. J. *Green Chem.* **2014**, *16*, 3132−3141.
(32) Wang, T.; Yuan, X.; Li, S.; Zeng, L.; Gong, J. *Nanoscale* **2015**, *7*, 7593−7602.
(33) Comotti, M.; Della Pina, C.; Matarrese, R.; Rossi, M. *Angew. Chem., Int. Ed.* **2004**, *43*, 5812−5815.
(34) Heidkamp, K.; Decker, N.; Martens, K.; Prüße, U.; Vorlop, K.-D.; Franke, O.; Stankowiak, A. *Eur. J. Lipid Sci. Technol.* **2010**, *112*, 51−57.
(35) Biella, S.; Prati, L.; Rossi, M. *J. Catal.* **2002**, *206*, 242−247.
(36) Casanova, O.; Iborra, S.; Corma, A. *ChemSusChem* **2009**, *2*, 1138−1144.
(37) Lo, C.-t. F.; Karan, K.; Davis, B. R. *Ind. Eng. Chem. Res.* **2007**, *46*, 5478−5484.
(38) Wang, R.; Sun, J.; Gao, L.; Xu, C.; Zhang, J.; Liu, Y. *Nanoscale* **2011**, *3*, 904−906.
(39) Shin, H.-J.; Kim, K. K.; Benayad, A.; Yoon, S.-M.; Park, H. K.; Jung, I.-S.; Jin, M. H.; Jeong, H.-K.; Kim, J. M.; Choi, J.-Y.; Lee, Y. H. *Adv. Funct. Mater.* **2009**, *19*, 1987−1992.
(40) Eschemann, T. O.; Lamme, W. S.; Manchester, R. L.; Parmentier, T. E.; Cognigni, A.; Rønning, M.; de Jong, K. P. *J. Catal.* **2015**, *328*, 130−138.
(41) Philippe Serp, B. M. *Nanostructured Carbon Materials for Catalysis*; Royal Society of Chemistry: London, 2015; p 555.
(42) Villa, A.; Wang, D.; Veith, G. M.; Vindigni, F.; Prati, L. *Catal. Sci. Technol.* **2013**, *3*, 3036−3041.
(43) Noh, J. S.; Schwarz, J. A. *J. Colloid Interface Sci.* **1989**, *130*, 157−164.
(44) Kundu, S.; Wang, Y.; Xia, W.; Muhler, M. *J. Phys. Chem. C* **2008**, *112*, 16869−16878.
(45) Martinez, M. T.; Callejas, M. A.; Benito, A. M.; Cochet, M.; Seeger, T.; Ansón, A.; Schreiber, J.; Gordon, C.; Marhic, C.; Chauvet, O.; Fierro, J. L. G.; Maser, W. K. *Carbon* **2003**, *41*, 2247−2256.
(46) Montes-Morán, M. A.; Suárez, D.; Menéndez, J. A.; Fuente, E. *Carbon* **2004**, *42*, 1219−1225.
(47) Watanabe, H.; Asano, S.; Fujita, S.-i.; Yoshida, H.; Arai, M. *ACS Catal.* **2015**, *5*, 2886−2894.
(48) Albonetti, S.; Lolli, A.; Morandi, V.; Migliori, A.; Lucarelli, C.; Cavani, F. *Appl. Catal., B* **2015**, *163*, 520−530.
(49) Casanova, O.; Iborra, S.; Corma, A. *ChemSusChem* **2009**, *2*, 1138−1144.
(50) Bartholomew, C. H. *Appl. Catal., A* **2001**, *212*, 17−60.
(51) Cao, A.; Lu, R.; Veser, G. *Phys. Chem. Chem. Phys.* **2010**, *12*, 13499−13510.
(52) Laveille, P.; Guillois, K.; Tuel, A.; Petit, C.; Basset, J.-M.; Caps, V. *Chem. Commun.* **2016**, *52*, 3179−3182.
(53) Lopez, N.; Nørskov, J. K.; Janssens, T. V. W.; Carlsson, A.; Puig-Molina, A.; Clausen, B. S.; Grunwaldt, J. D. *J. Catal.* **2004**, *225*, 86−94.
(54) Han, C. W.; Majumdar, P.; Marinero, E. E.; Aguilar-Tapia, A.; Zanella, R.; Greeley, J.; Ortalan, V. *Nano Lett.* **2015**, *15*, 8141−8147.
(55) Ait Rass, H.; Essayem, N.; Besson, M. *Green Chem.* **2013**, *15*, 2240−2251.
(56) Regalbuto, J. R. In *Synthesis of Solid Catalysts*; Jong, K. P., Ed.; Wiley-VCH: Weinheim, Germany, 2009; p 401.

DOI: 10.1021/acscatal.7b00829
ACS Catal. 2017, 7, 4581−4591